Article

Catalytic Application of Functionalized Bimetallic−Organic Frameworks with Phosphorous Acid Tags in the Synthesis of Pyrazolo[4,3-e]pyridines

Milad Mohammadi Rasooll, Hassan Sepehrmansourie, Mahmoud Zarei,* Mohammad Ali Zolfigol,* Mojtaba Hosseinifard, and Yanlong Gu

Read Online

ACCESS | Metrics & More | Article Recommendations | Supporting Information

ABSTRACT: Combining two different metals for the synthesis of a metal−organic framework (MOF) is a smart strategy for the architecture of new porous materials. Herein, a bimetal−organic framework (bimetal−MOFs) based on Fe and Co metals was synthesized. Then, phosphorous acid tags were decorated on bimetal−MOFs via a postmodification method as a new porous acidic functionalized catalyst. This catalyst was used for the synthesis of pyrazolo[4,3-e]pyridine derivatives as suitable drug candidates. The present study provides new insights into the architecture of novel porous heterogeneous catalysts based on a bimetal−organic framework (bimetal−MOFs). The type of final structures of catalyst and pyrazolo[4,3-e]pyridine derivatives were determined using different techniques such as fourier transform infrared (FT-IR), X-ray diffraction (XRD), scanning electron microscopy (SEM), energy-dispersive X-ray (EDX), SEM-elemental mapping, N_2 adsorption−desorption isotherm, Barrett−Joyner−Halenda (BJH), thermogravimetry/differential thermal analysis (TG/DTA), ^1H NMR, and ^{13}C NMR.
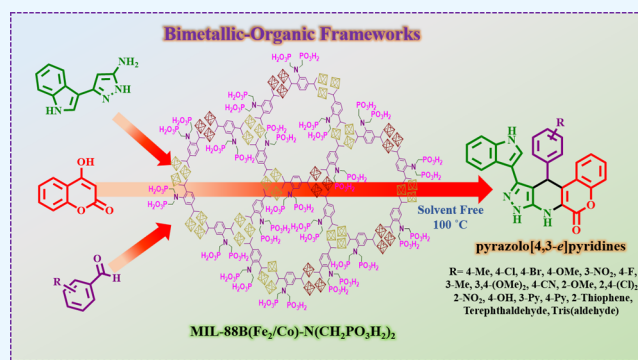
INTRODUCTION

In recent years, porous materials, including metal−organic frameworks (MOFs), Santa Barbara amorphous-15 (SBA-15), zeolites, and covalent organic frameworks (COFs), have gained significant attention as chemical nanoreactors. MOFs, in particular, are synthesized by combining metal clusters and organic compounds as nuclei and ligands, respectively. These materials offer unique properties and structures that make them highly attractive for various applications as catalysts, gas storage, and separation processes.[1−6] It is known that two-dimensional (2D) and three-dimensional (3D) porous structures have distinctive features such as tunable pore size, diverse structure, large surface area, and tunable chemistry.[7−9] Metal−organic frameworks are widely used in various fields such as gas separation, drug delivery, energy storage, and catalyst.[10−14] Also, the catalytic activities of metal−organic frameworks include photocatalysis,[15,16] asymmetric catalysis,[17,18] supramolecular catalysis,[19,20] oxidation of materials,[21] biomass conversion,[22,23] electrocatalysis,[24,25] acidic and basic catalysis,[26−38] separation of toxic substances from different phases, medical, biological, sensors, and solar cells.[39,40] Metal−organic frameworks based on a combination of two metals have better stability and properties than single-metal MOFs.[41−44] The synergistic effect achieved by incorporating two metals in bimetallic MOFs can significantly enhance their

catalytic activity. As a result, the synthesis of bimetallic MOFs has emerged as an attractive approach in this field, offering new avenues for exploration. The molar ratios of the metal components in MOFs can be readily adjusted to control the composition of bimetallic MOFs. This control allows for the creation of unique properties and characteristics in these compounds, addressing the limitations and deficiencies observed in monometallic MOFs. Through this method, bimetallic MOFs offer the potential to overcome these challenges and enhance the performance of catalytic systems.[45−47]

The postmodification method has been considered for designing various catalysts based on metal−organic frameworks (MOFs). In this method, MOFs are assembled and modified with various chemical reagents while their structure and network remain intact.[26−37] Our research groups have introduced a new category of acidic catalysts and/or reagents
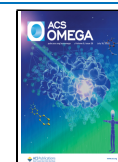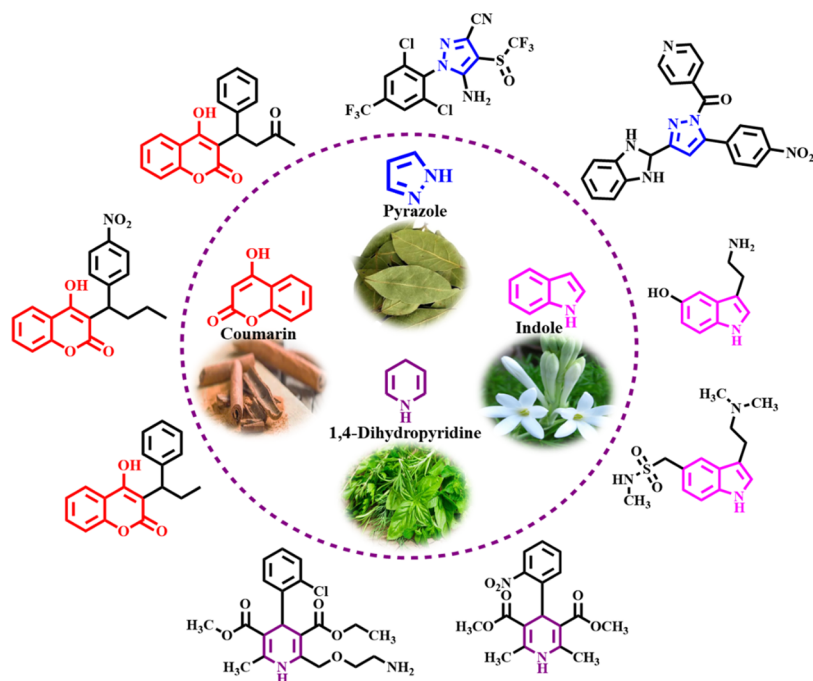
Figure 1. Few medicinal and biological compounds containing indole, pyrazole, coumarin, and 1,4-dihydropyran moieties.

via a postmodification methodology for inserting phosphorous acid tags on the surface of metal−organic frameworks,[26−32] mesopores,[48,49] melamine,[50] carbon quantum dots,[51,52] glycoluril,[53] and uric acid.[54] Phosphorous acid as a catalyst has been used for the oligomerization of light olefins, destructive alkylation of hydrocarbons, and organic synthesis.[55] Furthermore, phosphorous acid and its derivatives have been also used in multinuclear NMR, adsorption, and extraction.[56] Materials containing $N(CH_2PO_3H_2)_2$ moieties have environmental impacts worldwide in agricultural, chemical, and pharmaceutical applications.[57]

Research and development (R&D) is necessary for the synthesis of organic compounds without using toxic chemicals, hazardous solvents, easy reaction conditions, etc.[58,59] Catalytic reactions are one of the most important categories of dominant reactions in the synthesis of fine chemicals, bioactive materials, and pharmaceuticals. Due to the stability, porosity, and suitable surface of the designed and synthesized catalysts based on bimetallic MOFs, their catalytic activity is very suitable.[60,61] N-Heterocycle compounds such as pyrazolo[4,3-e]pyridine structures are an important class of organic compounds with unique medicinal and biological properties.[62,63] Also, scaffolds based on indole, pyrazole, coumarin, and 1,4-dihydropyran moieties have been studied in various pharmaceutical fields as antitumor, painkiller, antihypertensive, anti-inflammatory, antifungal, and antimicrobial drugs (Figure 1).[64−68]

In this study, we have embraced the principles of green chemistry to develop and present an efficient strategy for synthesizing pyrazolo[4,3-e]pyridines incorporating indole, pyrazole, coumarin, and 1,4-dihydropyran moieties. To accomplish this objective, we employed MIL-88B(Fe₂/Co)-$N(CH_2PO_3H_2)_2$ as a porous catalyst, which was achieved through the postmodification of metal−organic frameworks using bimetal Fe and Co. The incorporation of these two metals in the catalyst structure enhances its stability and imparts synergistic properties that contribute to its overall performance.

■ EXPERIMENTAL SECTION

Materials and Methods. FeCl₃·6H₂O (Sigma-Aldrich, 99%), Co(NO₃)₃·6H₂O (Sigma-Aldrich, 99%), 2-amino-

Scheme 1. Preparation of MIL-88B(Fe₂/Co)-N(CH₂PO₃H₂)₂ as a New Porous Catalyst
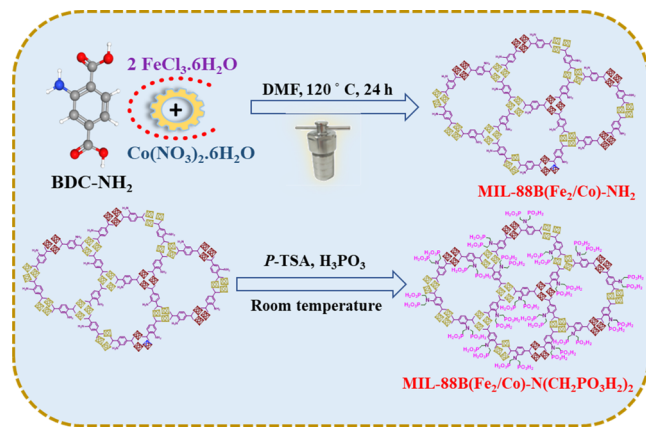
terephthalic acid (NH₂-BDC, 95%), hydrazine (N₂H₄, 80%), indole (C₈H₇N, 99%), cyanoacetic acid (C₃H₃NO₂, 99%), acetic anhydride (C₄H₆O₃, 95%), and various aromatic aldehydes (95%) were purchased from Merck and Sigma-Aldrich. Furthermore, ethanol (EtOH, 99%), acetonitrile (CH₃CN, 99%), N,N-dimethylformamide (DMF, 99%), methanol (MeOH, 99%), and other solvents were purchased from commercial sources without further purification. The Fourier transform infrared (FT-IR) technique model device (PerkinElmer Spectrum Version 10.02.00) was used to identify the functional groups of the different stages of catalyst. Moreover, the morphology of the different stages of the catalyst was characterized using the scanning electron microscopy (SEM) technique (TESCAN MIRA-II, Czechia). In addition, the thermal and chemical stability of the catalyst

Scheme 2. Synthesis of Pyrazolo[4,3-*e*]pyridine Derivatives Using MIL-88B(Fe₂/Co)-N(CH₂PO₃H₂)₂ as a New Porous Catalyst
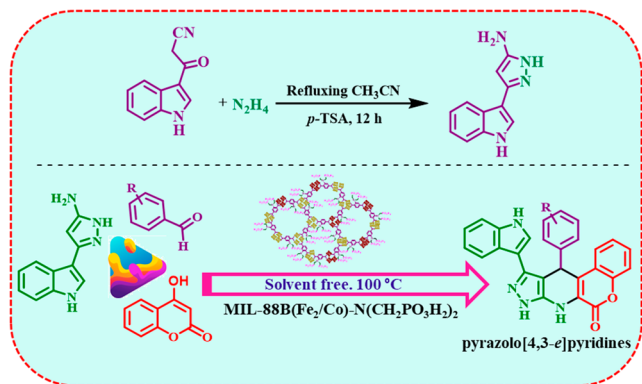
was determined using the thermogravimetry/differential thermal analysis (TG/DTA) technique (BAHR STA 503). Meanwhile, X-ray powder diffraction (XRD) technique with a model device PHILIPS PW1730 (Netherlands) energy-dispersive spectroscopy (EDS) and elemental mapping was carried out by the model TESCAN MIRA-II (Czechia) and Sigma VP ZEISS (German). Finally, Brunauer−Emmett−Teller (BET, BELSORP-mini-II) British Journal of Haematology (BJH) technique with a model device BELSORP-mini-II was utilized to determine the surface area and pore size of the synthesized catalyst.

Preparation of MIL-88B(Fe₂/Co)-NH₂. For the synthesis of the desired bimetal−organic framework (bimetal−MOFs), a mixture of FeCl₃·6H₂O (1.33 mmol, 0.359 g), Co(NO₃)₃·6H₂O (0.66 mmol, 0.192 g), and DMF (7.5 mL) was stirred in a round-bottom flask (20 mL) as solution 1. In another 10 mL flask, NH₂-BDC (2 mmol, 0.362 g) in 7.5 mL of DMF was dissolved as solution 2. Then, solution 1 was added to solution 2 and stirred at room temperature for 60 min. After this time, the resulting mixture was poured into a Teflon-lined bomb (60 mL) and placed in an oven at 120 °C for 24 h. In the following, a brown solid was separated by centrifugation and washed with DMF and EtOH several times. Then, MIL-88B(Fe₂/Co)-NH₂ was placed in an oven at 100 °C for 12 h.[69]

Preparation of MIL-88B(Fe₂/Co)-N(CH₂PO₃H₂)₂ as a New Porous Catalyst. In a 20 mL round-bottom flask, a mixture of MIL-88B(Fe₂/Co)-NH₂ (0.5 g), phosphorous acid (2 mmol, 0.164 g), paraformaldehyde (3 mmol, 0.09 g), *p*-TSA (10 mol %, 0.017 g), and dry EtOH (50 mL) as solvent was stirred for 12 h at room temperature. After this time, MIL-88B(Fe₂/Co)-N(CH₂PO₃H₂)₂ as a new bimetal−organic framework (bimetal−MOFs) was separated by centrifugation and washed with ethanol two times (Scheme 1).

General Procedure for the Synthesis of Pyrazolo[4,3-*e*]pyridines. The catalytic application of MIL-88B(Fe₂/Co)-N(CH₂PO₃H₂)₂ as an efficient heterogeneous and porous catalyst functionalized with phosphorous acid tags in the preparation of pyrazolo[4,3-*e*]pyridine derivatives was investigated. In this regard, 3-(cyanoacetyl)indole and 5-(1*H*-Indol-3-yl)-2*H*-pyrazol-3-ylamine were synthesized according to the previously reported methodology (Scheme 2).[68] Then, in a 10 mL round-bottom flask, a mixture of 5-(1*H*-indol-3-yl)-2*H*-pyrazol-3-ylamine (1 mmol, 0.198 g), 4-hydroxy-2*H*-chromen-2-one (1 mmol, 0.162 g), benzaldehyde derivatives (1 mmol), and 10 mg of MIL-88B(Fe₂/Co)-N(CH₂PO₃H₂)₂ as a porous

catalyst was added and stirred under solvent-free conditions at 100 °C. The progress of the reaction was followed by the TLC technique. Afterward, the reaction mixture was added to hot EtOH (20 mL) and the presented catalyst was separated by centrifugation (1000 rpm, 5 min). The precipitate was washed with cold EtOH to obtain the desired pure product (Scheme 2).

Spectral Data. *410-(1H-Indol-3-yl)-11-(p-tolyl)-8,11-dihydrochromeno[3,4-b]pyrazolo[4,3-e]pyridin-6(7H)-one (K1).* Yellow solid; mp: >300 °C; FT-IR (KBr, cm⁻¹): 3288, 3057, 1646, 1611, 1561. ¹H NMR (400 MHz, DMSO-*d₆*) δ$_{ppm}$ 12.54 (s, 1H), 11.54 (s, 1H), 10.77 (s, 1H), 8.52 (d, *J* = 7.9 Hz, 1H), 7.84 (d, *J* = 7.9 Hz, 1H), 7.72 (t, *J* = 7.9 Hz, 1H), 7.52 (t, *J* = 7.3 Hz, 2H), 7.47−7.42 (m, 2H), 7.27 (t, *J* = 7.5 Hz, 1H), 7.20 (t, *J* = 7.5 Hz, 1H), 7.11 (d, 2H), 7.01 (d, *J* = 8.1 Hz, 2H), 5.45 (s, 1H), 2.23 (s, 3H). ¹³C NMR (101 MHz, DMSO-*d₆*) δ$_{ppm}$ 160.71, 151.95, 146.92, 144.06, 143.82, 135.81, 134.81, 134.11, 131.56, 128.38, 127.41, 124.55, 123.75, 123.03, 121.78, 119.60, 119.52, 116.58, 114.04, 111.78, 104.24, 101.17, 97.80, 36.43, 20.48.

11-(4-Chlorophenyl)-10-(1H-indol-3-yl)-8,11-dihydrochromeno[3,4-b]pyrazolo[4,3-e]pyridin-6(7H)-one (K2). White solid; mp: >300 °C; FT-IR (KBr, cm⁻¹): 3290, 3063, 1649, 1612, 1552. ¹H NMR (400 MHz, DMSO-*d₆*) δ$_{ppm}$ 12.50 (s, 1H), 11.47 (s, 1H), 10.76 (s, 1H), 8.43 (d, *J* = 8.2 Hz, 1H), 7.70 (d, *J* = 7.9 Hz, 1H), 7.65−7.60 (m, 1H), 7.46−7.39 (m, 2H), 7.38−7.34 (m, 2H), 7.19−7.12 (m, 3H), 7.12−7.07 (m, 3H), 5.41 (s, 1H). ¹³C NMR (101 MHz, DMSO-*d₆*) δ$_{ppm}$ 160.7, 152.0, 146.7, 145.6, 144.4, 135.8, 134.3, 131.7, 130.3, 129.3, 127.7, 124.7, 123.8, 123.1, 121.8, 119.6, 119.4, 116.6, 113.9, 111.8, 104.0, 100.7, 97.0, 36.5.

11-(4-Bromophenyl)-10-(1H-indol-3-yl)-8,11-dihydrochromeno[3,4-b]pyrazolo[4,3-e]pyridin-6(7H)-one (K3). White solid; mp: >300 °C; FT-IR (KBr, cm⁻¹): 3468, 3165, 1672, 1611, 1507. ¹H NMR (400 MHz, DMSO-*d₆*) δ$_{ppm}$ 12.50 (s, 1H), 11.47 (s, 1H), 10.76 (s, 1H), 8.43 (d, *J* = 8.2 Hz, 1H), 7.70 (d, *J* = 7.9 Hz, 1H), 7.65−7.60 (m, 1H), 7.46−7.40 (m, 2H), 7.39−7.34 (m, 2H), 7.30−7.25 (m, 2H), 7.17 (t, *J* = 6.9 Hz, 1H), 7.12−7.02 (m, 3H), 5.40 (s, 1H). ¹³C NMR (101 MHz, DMSO-*d₆*) δ$_{ppm}$ 160.7, 152.0, 146.7, 146.0, 144.4, 135.8, 134.4, 131.7, 130.6, 129.7, 124.7, 123.8, 123.1, 121.8, 119.7, 119.4, 118.9, 116.7, 114.0, 111.8, 104.0, 100.7, 97.0, 36.5.

10-(1H-Indol-3-yl)-11-(4-methoxyphenyl)-8,11-dihydrochromeno[3,4-b]pyrazolo[4,3-e]pyridin-6(7H)-one (K4). Yellow solid; mp: >300 °C; FT-IR (KBr, cm⁻¹): 3418, 3296, 1663, 1611. 1508. ¹H NMR (400 MHz, DMSO-*d₆*) δ$_{ppm}$ 12.55 (s, 1H), 11.55 (s, 1H), 10.77 (s, 1H), 8.53 (d, *J* = 6.9 Hz, 1H), 7.86 (d, *J* = 8.1 Hz, 1H), 7.75−7.70 (m, 1H), 7.53 (t, *J* = 7.9 Hz, 2H), 7.47−7.42 (m, 2H), 7.28 (t, *J* = 7.6 Hz, 1H), 7.21 (t, *J* = 6.9 Hz, 1H), 7.16 (d, 2H), 6.79 (d, *J* = 8.9 Hz, 2H), 5.44 (s, 1H), 3.72 (s, 3H). ¹³C NMR (101 MHz, DMSO-*d₆*) δ$_{ppm}$ 160.7, 157.3, 151.9, 147.0, 143.9, 139.0, 135.8, 134.1, 131.5, 128.5, 124.6, 124.5, 123.7, 123.0, 121.8, 119.6, 119.5, 116.6, 114.1, 113.2, 111.8, 104.3, 101.3, 98.0, 54.8, 36.0.

10-(1H-Indol-3-yl)-11-(3-nitrophenyl)-8,11-dihydrochromeno[3,4-b]pyrazolo[4,3-e]pyridin-6(7H)-one (K5). Brown solid; mp: >300 °C; FT-IR (KBr, cm⁻¹): 3421, 3264, 1706, 1672, 1613. ¹H NMR (400 MHz, DMSO-*d₆*) δ$_{ppm}$ 12.44 (s, 1H), 11.57 (s, 1H), 10.95 (s, 1H), 8.56 (d, *J* = 8.2 Hz, 1H), 7.97−7.93 (m, 2H), 7.76−7.72 (m, 2H), 7.65−7.62 (m, 1H), 7.58 (d, *J* = 2.7 Hz, 1H), 7.53−7.45 (m, 4H), 7.26 (t, 1H), 7.18 (t, *J* = 7.5 Hz, 1H), 5.70 (s, 1H). ¹³C NMR (101

MHz, DMSO-d_6) δ_{ppm} 172.0, 160.7, 152.1, 148.5, 147.1, 146.3, 144.8, 135.8, 134.2, 131.9, 129.2, 125.0, 124.8, 123.9, 123.2, 121.9, 121.8, 121.0, 119.6, 119.3, 116.7, 113.8, 111.8, 103.7, 100.4, 96.3, 37.0.

11-(4-Fluorophenyl)-10-(1H-indol-3-yl)-8,11-dihydrochromeno[3,4-b]pyrazolo[4,3-e]pyridin-6(7H)-one (K6). White solid; mp: >300 °C; FT-IR (KBr, cm⁻¹): 3473, 3256, 1667, 1615, 1511. ¹H NMR (400 MHz, DMSO-d_6) δ_{ppm} 12.57 (s, 1H), 11.54 (s, 1H), 10.83 (s, 1H), 8.53 (d, J = 8.2 Hz, 1H), 7.81 (d, J = 7.9 Hz, 1H), 7.71 (t, J = 7.1 Hz, 1H), 7.54–7.47 (m, 2H), 7.47–7.42 (m, 2H), 7.29–7.17 (m, 4H), 7.01 (t, J = 8.9 Hz, 2H), 5.51 (s, 1H). ¹³C NMR (101 MHz, DMSO-d_6) δ_{ppm} 161.5, 160.7, 159.1, 152.0, 146.7, 144.2, 142.9, 135.8, 134.3, 131.6, 129.2, 124.7, 124.6, 123.8, 123.1, 121.8, 119.6, 116.6, 114.3, 114.0, 111.8, 104.1, 101.0, 97.4, 36.2.

10-(1H-Indol-3-yl)-11-(m-tolyl)-8,11-dihydrochromeno-[3,4-b]pyrazolo[4,3-e]pyridin-6(7H)-one (K7). Yellow solid; mp: >300 °C; FT-IR (KBr, cm⁻¹): 3408, 3275, 1651, 1611, 1508. ¹H NMR (400 MHz, DMSO-d_6) δ_{ppm} 12.54 (s, 1H), 11.55 (s, 1H), 10.77 (s, 1H), 8.53 (d, J = 8.2 Hz, 1H), 7.81 (d, J = 7.8 Hz, 1H), 7.74–7.70 (m, 1H), 7.54 (d, J = 8.3 Hz, 1H), 7.52–7.48 (m, 1H), 7.45 (d, J = 8.3 Hz, 1H), 7.41 (d, J = 2.7 Hz, 1H), 7.27 (t, J = 8.1 Hz, 1H), 7.20 (t, J = 7.5 Hz, 1H), 7.09 (t, J = 7.5 Hz, 1H), 7.03–6.96 (m, 2H), 6.93 (d, J = 7.5 Hz, 1H), 5.44 (s, 1H), 2.18 (s, 3H). ¹³C NMR (101 MHz, DMSO-d_6) δ_{ppm} 160.7, 152.0, 146.7, 144.3, 136.6, 135.8, 134.1, 131.6, 128.0, 127.7, 126.6, 124.8, 124.6, 123.8, 123.1, 121.8, 119.6, 116.6, 114.1, 111.8, 104.2, 101.3, 97.5, 36.8, 21.0.

11-(3,4-Dimethoxyphenyl)-10-(1H-indol-3-yl)-8,11-dihydrochromeno[3,4-b]pyrazolo[4,3-e]pyridin-6(7H)-one (K8). Yellow solid; mp: >300 °C; FT-IR (KBr, cm⁻¹): 3362, 3171, 1666, 1611, 1568. ¹H NMR (400 MHz, DMSO-d_6) δ_{ppm} 12.47 (s, 1H), 11.58 (s, 1H), 10.75 (s, 1H), 8.51 (d, J = 8.2 Hz, 1H), 7.83 (d, J = 7.8 Hz, 1H), 7.71 (ddd, J = 8.5, 7.3, 1.4 Hz, 1H), 7.55 (d, J = 7.8 Hz, 1H), 7.52–7.44 (m, 3H), 7.30–7.26 (m, 1H), 7.25–7.20 (m, 1H), 6.77 (d, J = 8.4 Hz, 1H), 6.68 (d, J = 2.1 Hz, 1H), 6.59 (dd, J = 8.3, 2.1 Hz, 1H), 5.47 (s, 1H), 3.67 (s, 3H), 3.38 (s, 3H). ¹³C NMR (101 MHz, DMSO-d_6) δ_{ppm} 160.9, 152.0, 147.6, 146.7, 144.3, 139.4, 135.9, 134.2, 131.5, 123.8, 123.0, 121.8, 119.7, 119.5, 118.7, 116.6, 114.0, 111.8, 111.5, 111.4, 104.5, 101.5, 97.3, 55.2, 54.6, 36.3.

10-(1H-Indol-3-yl)-11-(pyridin-3-yl)-8,11-dihydrochromeno[3,4-b]pyrazolo[4,3-e]pyridin-6(7H)-one (K9). Yellow solid; mp: >300 °C; FT-IR (KBr, cm⁻¹): 3169, 1672, 1611, 1562, 1505. ¹H NMR (400 MHz, DMSO-d_6) δ_{ppm} 12.50 (s, 1H), 11.46 (s, 1H), 10.78 (s, 1H), 8.45 (d, J = 6.7 Hz, 1H), 8.30 (d, J = 2.4 Hz, 1H), 8.17 (dd, J = 4.8, 1.7 Hz, 1H), 7.70 (d, J = 7.7 Hz, 1H), 7.66–7.61 (m, 1H), 7.45 (d, J = 2.7 Hz, 1H), 7.44–7.39 (m, 3H), 7.36 (d, J = 8.2 Hz, 1H), 7.17 (t, J = 8.2 Hz, 1H), 7.11 (t, J = 3.6 Hz, 1H), 7.10–7.06 (m, 1H), 5.47 (s, 1H). ¹³C NMR (101 MHz, DMSO-d_6) δ_{ppm} 160.8, 152.1, 148.4, 146.9, 146.5, 144.7, 141.8 135.8, 135.0, 134.6, 131.9, 124.8, 124.7, 123.9, 123.4, 123.2, 121.9, 119.7, 119.4, 116.7, 113.8, 111.9, 103.9, 100.4, 96.5, 34.8.

4-(10-(1H-Indol-3-yl)-6-oxo-6,7,8,11-tetrahydrochromeno[3,4-b]pyrazolo[4,3-e]pyridin-11-yl)-benzonitrile (K10). White solid; mp: >300 °C; FT-IR (KBr, cm⁻¹): 3338, 3171, 2223, 1672, 1611. ¹H NMR (400 MHz, DMSO-d_6) δ_{ppm} 12.63 (s, 1H), 11.57 (s, 1H), 10.93 (s, 1H), 8.55 (d, J = 8.2 Hz, 1H), 7.79–7.72 (m, 2H), 7.64 (d, J = 8.3 Hz, 2H), 7.55–7.50 (m, 3H), 7.47 (d, J = 8.2 Hz, 1H), 7.35 (d, J = 8.3 Hz, 2H), 7.28 (t, J = 7.6 Hz, 1H), 7.20 (t, J = 7.5 Hz, 1H), 5.61 (s, 1H). ¹³C NMR (101 MHz, DMSO-d_6) δ_{ppm}

160.7, 151.9, 146.5, 144.7, 135.8, 134.6, 131.8, 128.5, 124.8, 124.7, 123.9, 123.2, 121.8, 119.7, 119.3, 118.8, 116.7, 113.9, 111.8, 108.6, 103.8, 100.3, 96.4, 37.3.

10-(1H-Indol-3-yl)-11-(2-methoxyphenyl)-8,11-dihydrochromeno[3,4-b]pyrazolo[4,3-e]pyridin-6(7H)-one (K11). Yellow solid; mp: >300 °C; FT-IR (KBr, cm⁻¹): 3416, 3304, 1654, 1611, 1567. ¹H NMR (400 MHz, DMSO-d_6) δ_{ppm} 12.35 (s, 1H), 11.54 (s, 1H), 10.70 (s, 1H), 8.55 (d, J = 6.9 Hz, 1H), 7.78–7.70 (m, 2H), 7.55–7.50 (m, 2H), 7.48–7.43 (m, 2H), 7.26 (t, 1H), 7.20–7.14 (m, 2H), 7.12–7.07 (m, 1H), 6.85 (d, J = 7.4 Hz, 1H), 6.80 (t, J = 7.5 Hz, 1H), 5.78 (s, 1H), 3.49 (s, 3H). ¹³C NMR (101 MHz, DMSO-d_6) δ_{ppm} 160.4, 156.0, 152.0, 147.0, 144.8, 135.8, 135.3, 133.8, 131.4, 129.5, 127.0, 125.1, 124.9, 123.6, 123.0, 121.5, 120.0, 119.5, 119.4, 116.5, 114.1, 111.6, 111.18, 104.2, 101.6, 97.4, 31.4.

11-(2,4-Dichlorophenyl)-10-(1H-indol-3-yl)-8,11-dihydrochromeno[3,4-b]pyrazolo[4,3-e]pyridin-6(7H)-one (K12). White solid; mp: >300 °C; FT-IR (KBr, cm⁻¹): 3419, 3264, 1678, 1612, 1562. ¹H NMR (400 MHz, DMSO-d_6) δ_{ppm} 12.52 (s, 1H), 11.54 (s, 1H), 10.77 (s, 1H), 8.51 (d, J = 6.9 Hz, 1H), 7.82 (d, J = 7.9 Hz, 1H), 7.73–7.68 (m, 1H), 7.53–7.47 (m, 2H), 7.44 (dd, J = 8.2, 1.2 Hz, 1H), 7.41 (d, J = 2.7 Hz, 1H), 7.26 (t, J = 8.1 Hz, 1H), 7.16–7.12 (m, 2H), 7.08 (d, J = 8.3 Hz, 2H), 5.44 (s, 1H).

10-(1H-Indol-3-yl)-11-(2-nitrophenyl)-8,11-dihydrochromeno[3,4-b]pyrazolo[4,3-e]pyridin-6(7H)-one (K13). Brown solid; mp: >300 °C; FT-IR (KBr, cm⁻¹): 3430, 3165, 3123, 1672, 1613, 1568. ¹H NMR (400 MHz, DMSO-d_6) δ_{ppm} 12.55 (s, 1H), 11.38 (s, 1H), 10.84 (s, 1H), 8.44 (d, J = 6.7 Hz, 1H), 7.72 (d, J = 8.2 Hz, 1H), 7.64–7.55 (m, 2H), 7.53–7.48 (m, 1H), 7.41 (d, J = 7.1 Hz, 1H), 7.38–7.34 (m, 2H), 7.33–7.26 (m, 3H), 7.12 (t, J = 7.6 Hz, 1H), 7.01 (t, J = 7.5 Hz, 1H), 6.20 (s, 1H). ¹³C NMR (101 MHz, DMSO-d_6) δ_{ppm} 160.8, 151.9, 148.1, 144.3, 140.6, 135.7, 133.1, 131.9, 127.2, 125.1, 125.0, 123.9, 123.5, 123.2, 121.7, 119.5, 119.3, 116.7, 113.7, 111.6, 103.5, 99.7, 96.9, 31.7.

11-(4-Hydroxyphenyl)-10-(1H-indol-3-yl)-8,11-dihydrochromeno[3,4-b]pyrazolo[4,3-e]pyridin-6(7H)-one (K14). Yellow solid; mp: >300 °C; FT-IR (KBr, cm⁻¹): 3356, 3246, 1644, 1611, 1551. ¹H NMR (400 MHz, DMSO-d_6) δ_{ppm} 12.41 (s, 1H), 11.42 (s, 1H), 10.62 (s, 1H), 9.09 (s, 1H), 8.41 (d, J = 7.4 Hz, 1H), 7.75 (d, J = 7.9 Hz, 1H), 7.63–7.57 (m, 1H), 7.44–7.36 (m, 2H), 7.34 (d, J = 8.3 Hz, 1H), 7.25 (d, J = 2.7 Hz, 1H), 7.17 (t, J = 7.0 Hz, 1H), 7.09 (t, J = 7.0 Hz, 1H), 6.94 (d, J = 8.6 Hz, 2H), 6.51 (d, J = 8.6 Hz, 2H), 5.25 (s, 1H). ¹³C NMR (101 MHz, DMSO-d_6) δ_{ppm} 160.9, 155.3, 151.9, 143.9, 137.4, 135.8, 131.6, 128.5, 124.6, 124.5, 123.8, 123.0, 121.9, 119.7, 119.5, 116.6, 114.6, 114.1, 111.8, 104.3, 101.5, 98.2, 35.9.

10-(1H-Indol-3-yl)-11-(2H-1λ4-thiophen-2-yl)-8,11-dihydrochromeno[3,4-b]pyrazolo[4,3-e]pyridin-6(7H)-one (K15). Black solid; mp: >300 °C; FT-IR (KBr, cm⁻¹): 3328, 1700, 1651, 1611, 1560. ¹H NMR (400 MHz, DMSO-d_6) δ_{ppm} 12.28 (s, 1H), 11.48 (s, 1H), 10.77 (s, 1H), 8.40 (d, J = 8.2 Hz, 1H), 7.80 (d, J = 8.1 Hz, 1H), 7.64 (t, J = 7.8 Hz, 1H), 7.45 (d, J = 7.0 Hz, 1H), 7.42–7.37 (m, 3H), 7.21–7.16 (m, 1H), 7.15–7.09 (m, 2H), 6.77–6.74 (m, 1H), 6.72–6.69 (m, 1H), 5.73 (s, 1H). ¹³C NMR (101 MHz, DMSO-d_6) δ_{ppm} 161.0, 151.9, 150.8, 144.1, 135.9, 131.9, 126.4, 124.6, 124.6, 124.0, 123.9, 123.3, 123.0, 121.9, 119.8, 119.4, 116.7, 113.9, 111.9, 104.3, 100.5, 97.0, 31.8.

10-(1H-Indol-3-yl)-11-(pyridin-4-yl)-8,11-dihydrochromeno[3,4-b]pyrazolo[4,3-e]pyridin-6(7H)-one

(K16). Yellow solid; mp: >300 °C; FT-IR (KBr, cm^{-1}): 3164, 1671, 1611, 1562, 1506. ^{1}H NMR (400 MHz, DMSO-d_6) δ_{ppm} 12.52 (s, 1H), 11.47 (s, 1H), 10.80 (s, 1H), 8.45 (d, J = 6.9 Hz, 1H), 8.24 (d, J = 6.2 Hz, 2H), 7.69−7.66 (m, 1H), 7.66−7.60 (m, 1H), 7.45−7.39 (m, 3H), 7.37 (dd, J = 8.3, 1.2 Hz, 1H), 7.17 (t, J = 7.0 Hz, 1H), 7.10 (t, J = 6.9 Hz, 1H), 7.02 (d, J = 6.2 Hz, 2H), 5.44 (s, 1H). ^{13}C NMR (101 MHz, DMSO-d_6) δ_{ppm} 160.8, 154.6, 152.1, 149.0, 146.5, 145.0, 135.8, 134.6, 132.0, 124.8, 124.7, 123.9, 123.2, 122.8, 121.9, 119.7, 119.3, 116.7, 113.8, 111.9, 103.8, 99.9, 95.9, 36.7.

11,11′-(1,4-Phenylene)bis(10-(1H-indol-3-yl)-8,11-dihydrochromeno[3,4-b]pyrazolo[4,3-e]pyridin-6(7H)-one) (K17). Yellow solid; mp: >300 °C; FT-IR (KBr, cm^{-1}): 3408, 3281, 1676, 1612, 1583. ^{1}H NMR (400 MHz, DMSO-d_6) δ_{ppm} 12.38 (s, 2H), 11.26 (d, J = 42.0 Hz, 2H), 10.59 (d, J = 5.0 Hz, 2H), 8.36 (d, J = 12.8 Hz, 2H), 7.61−7.51 (m, 4H), 7.41 (d, J = 8.2 Hz, 1H), 7.38−7.33 (m, 3H), 7.28 (t, J = 8.7 Hz, 2H), 7.15−7.08 (m, 2H), 7.06 (dd, J = 9.0, 2.6 Hz, 3H), 7.01−6.97 (m, 1H), 6.92−6.90 (m, 4H), 5.17 (d, J = 3.1 Hz, 2H). ^{13}C NMR (101 MHz, DMSO-d_6) δ_{ppm} 160.7, 151.9, 144.6, 144.4, 144.3, 136.3, 135.8, 135.7, 131.5, 127.1, 124.8, 124.3, 123.7, 123.0, 121.7, 119.5, 116.6, 114.0, 111.7, 104.2, 101.4, 97.6, 36.3.

11,11′,11″-(((1,3,5-Triazine-2,4,6-triyl)tris(oxy))tris(benzene-4,1-diyl))tris(10-(1H-indol-3-yl)-8,11-dihydrochromeno[3,4-b]pyrazolo[4,3-e]pyridin-6(7H)-one) (K18). Yellow solid; mp: >300 °C; FT-IR (KBr, cm^{-1}): 3276, 1680, 1612, 1563, 1502. ^{1}H NMR (400 MHz, DMSO-d_6) δ_{ppm} 12.45 (s, 3H), 11.40 (s, 3H), 10.71 (s, 3H), 8.41 (d, J = 8.5 Hz, 3H), 7.71−7.67 (m, 3H), 7.62−7.57 (m, 4H), 7.40−7.38 (m, 5H), 7.33−7.30 (m, 5H), 7.14−7.10 (m, 7H), 7.10−7.07 (m, 6H), 6.93−6.88 (m, 6H), 5.38 (s, 3H). ^{13}C NMR (101 MHz, DMSO-d_6) δ_{ppm} 172.8, 160.8, 152.0, 149.2, 144.5, 144.4, 135.8, 131.7, 128.5, 128.4, 124.6, 123.8, 123.1, 121.8, 120.9, 119.7, 116.7, 114.6, 114.0, 111.8, 101.0, 97.3, 36.3.

RESULTS AND DISCUSSION

Catalyst Preparation Strategy. Based on the concept of the modified strategy of MOFs in the design and synthesis of new catalysts in our group research,[26−37] we have presented a
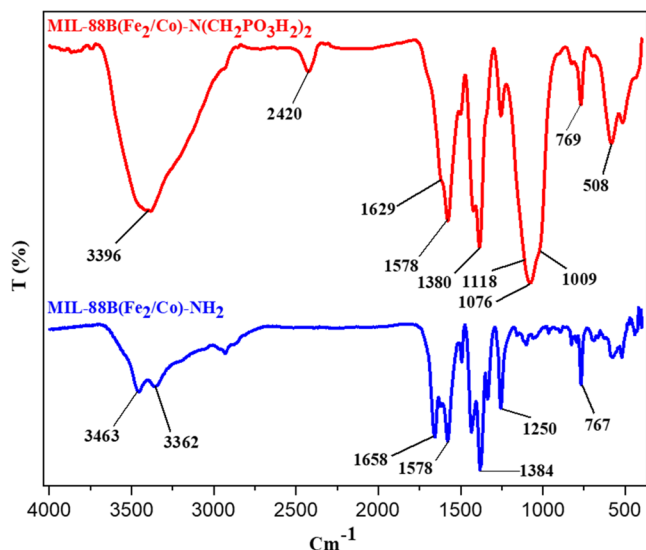

Figure 2. FT-IR spectra of MIL-88B(Fe$_2$/Co)-NH$_2$ and MIL-88B(Fe$_2$/Co)-N(CH$_2$PO$_3$H$_2$)$_2$.
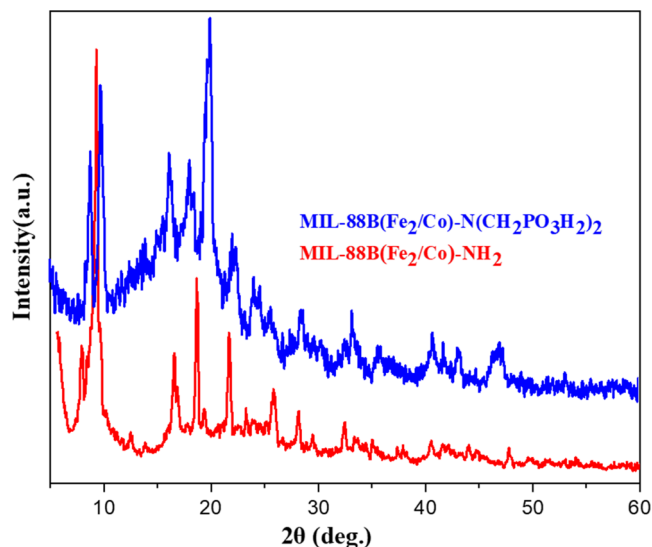
Figure 3. XRD of MIL-88B(Fe$_2$/Co)-NH$_2$ and MIL-88B(Fe$_2$/Co)-N(CH$_2$PO$_3$H$_2$)$_2$.
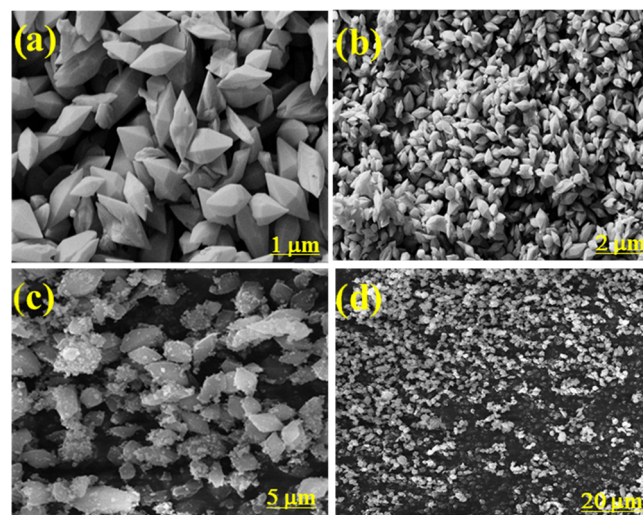
Figure 4. SEM images of MIL-88B(Fe$_2$/Co)-NH$_2$ (a, b) and MIL-88B(Fe$_2$/Co)-N(CH$_2$PO$_3$H$_2$)$_2$ (c, d).

new porous catalyst based on bimetal−organic frameworks (bimetal−MOFs). In the following, phosphorous acid tags have been used to decorate the bimetallic−organic frameworks, which have created acidic sites for increasing their catalytic activity. The strategy preparation of MIL-88B(Fe$_2$/Co)-N(CH$_2$PO$_3$H$_2$)$_2$ as a new porous catalyst is shown in Scheme 1. The structure of the catalyst was approved by various techniques such as FT-IR, XRD, energy-dispersive X-ray (EDX), elemental mapping, TG/DTA, SEM, N$_2$ adsorption−desorption isotherms (BET), and BJH analysis. Then, the catalytic activity of MIL-88B(Fe$_2$/Co)-N-(CH$_2$PO$_3$H$_2$)$_2$ was investigated in the preparation of pyrazolo-[4,3-e]pyridine derivatives with indole, pyrazole, coumarin, and 1,4-dihydropyran moieties with biological activity under solvent-free conditions at 100 °C (Scheme 2). The final structure of the products was confirmed using melting point, FT-IR, ^{1}H NMR, and ^{13}C NMR techniques.

Characterization. After the successful synthesis of MIL-88B(Fe$_2$/Co)-N(CH$_2$PO$_3$H$_2$)$_2$ as a new porous catalyst, the structure and morphology of MIL-88B(Fe$_2$/Co)-NH$_2$ and
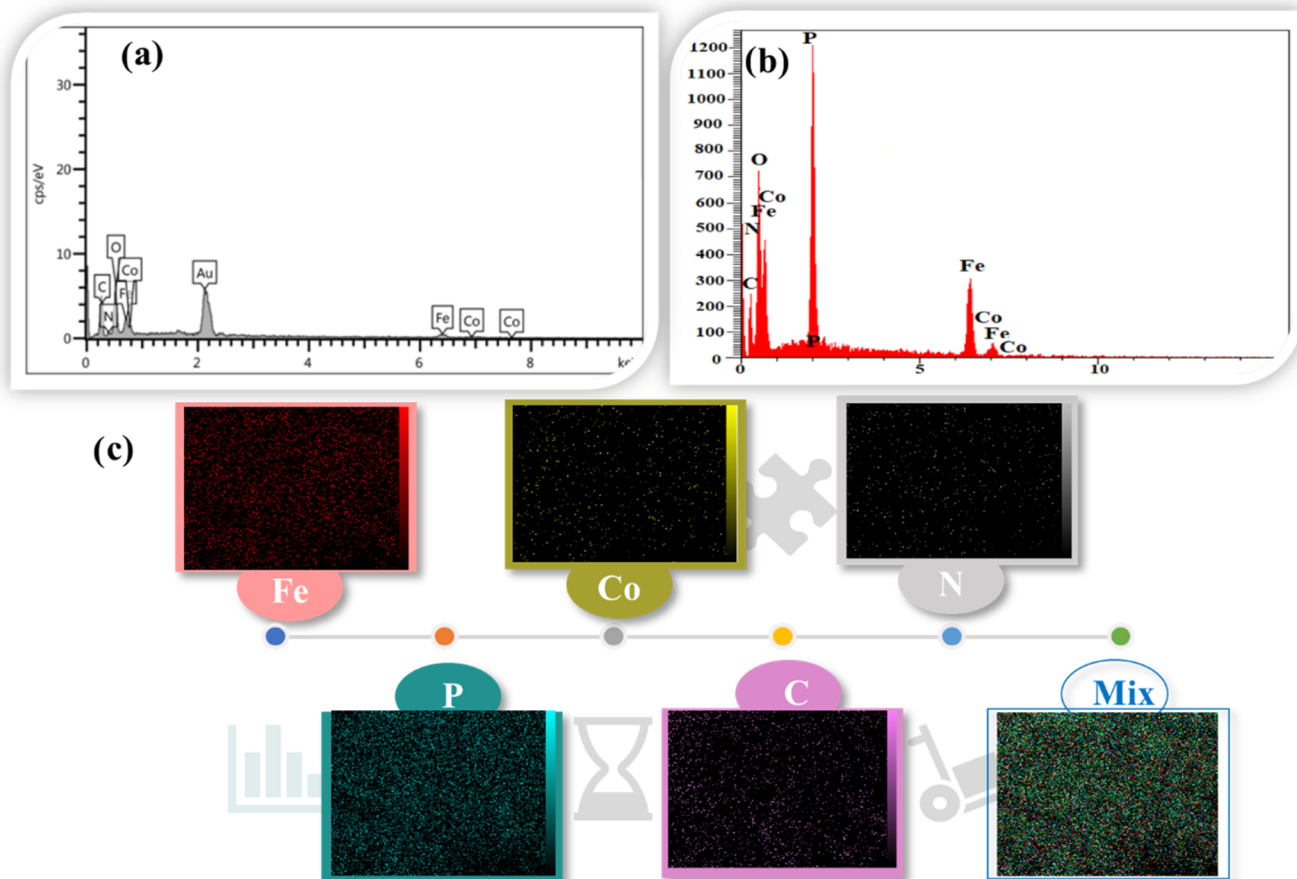
Figure 5. Energy-dispersive X-ray analysis (EDX) of MIL-88B(Fe$_2$/Co)-NH$_2$ and MIL-88B(Fe$_2$/Co)-N(CH$_2$PO$_3$H$_2$)$_2$ (a, b) and SEM elemental mapping of MIL-88B(Fe$_2$/Co)-N(CH$_2$PO$_3$H$_2$)$_2$ (c).
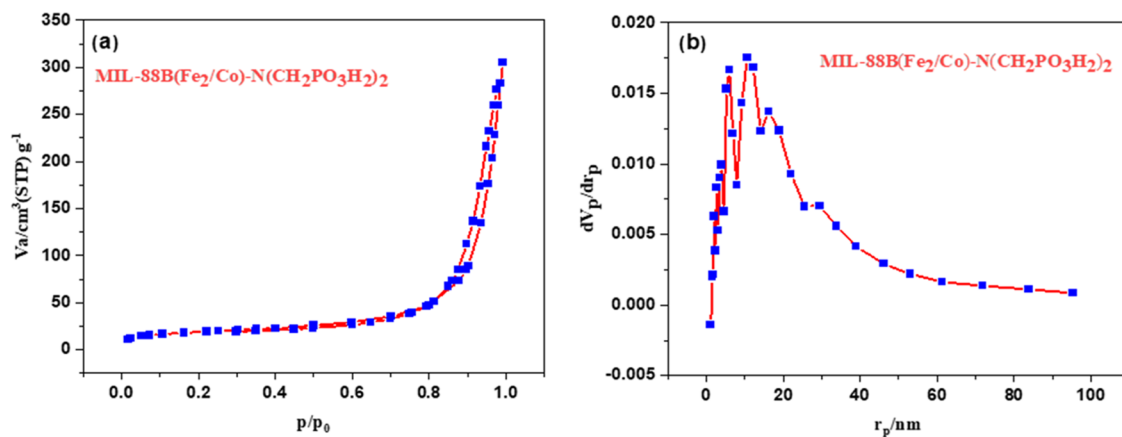

Figure 6. (a) N$_2$ adsorption−desorption isotherm and (b) pore size distribution plot based on the BJH method for MIL-88B(Fe$_2$/Co)-N(CH$_2$PO$_3$H$_2$)$_2$.

MIL-88B(Fe$_2$/Co)-N(CH$_2$PO$_3$H$_2$)$_2$ were investigated to confirm scaffolds of porous catalyst. Therefore, the FT-IR technique was used to confirm the functional groups of bimetal−MOF and the final catalyst. The peaks at 1658 and 1629 cm^{-1} indicate the vibration of C=O group in MIL-88B(Fe$_2$/Co)-NH$_2$ and MIL-88B(Fe$_2$/Co)-N(CH$_2$PO$_3$H$_2$)$_2$, respectively. Also, the peak at 769 cm^{-1} is related to the Fe−O and Co−O bond, which shows the binding of ligands to metals. The bifurcated peaks at 3362 and 3463 cm^{-1} indicate the NH$_2$ functional group, which has disappeared in the

structure of the final catalyst. Finally, the peaks at 1009, 1076, and 1118 cm^{-1} indicate P=O and P−O bonds in phosphorus acid tags (Figure 2).

The crystalline structure of the obtained MIL-88B(Fe$_2$/Co)-N(CH$_2$PO$_3$H$_2$)$_2$ as a new porous catalyst was studied by the XRD technique (Figure 3). The crystal pattern of MIL-88B(Fe$_2$/Co)-NH$_2$ is in good agreement with the previous report.[69] The crystal pattern of MIL-88B(Fe$_2$/Co)-N-(CH$_2$PO$_3$H$_2$)$_2$ shows that the early-stage crystal plates were not destroyed in the course of synthesis. The new peaks that
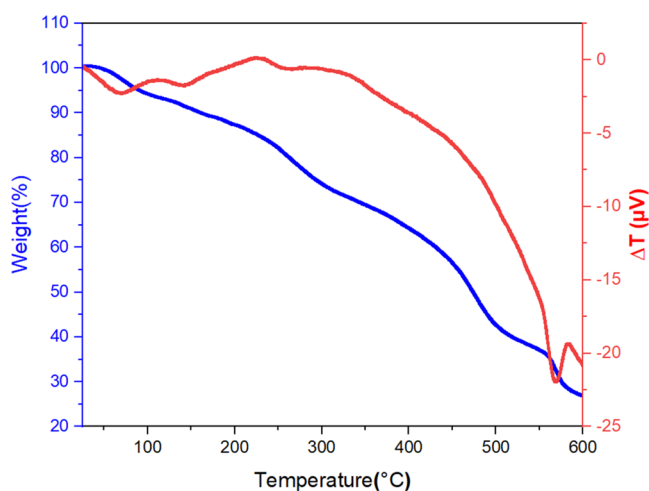
Figure 7. Thermal gravimetric (TG) and differential thermal analysis (DTA) of MIL-88B(Fe$_2$/Co)-N(CH$_2$PO$_3$H$_2$)$_2$.

emerged in the second stage are related to the formation of phosphorous acid during the synthesis of the target catalyst. The changes made well indicate the formation of the desired catalyst along with the stability of its crystalline plates.

The morphology of bimetal−MOF as well as MIL-88B(Fe$_2$/Co)-N(CH$_2$PO$_3$H$_2$)$_2$ was determined using the SEM technique (Figure 4). The morphology of MIL-88B(Fe$_2$/Co)-NH$_2$ showed a spindle-like structure (Figure 4a,b). Also, the structure of MIL-88B(Fe$_2$/Co)-NH$_2$ functionalized with

phosphorous acid tags was confirmed by SEM images, which shows that the morphology is stable (Figure 4c,d).

The presence and distribution of elements in MIL-88B(Fe$_2$/Co)-NH$_2$ and MIL-88B(Fe$_2$/Co)-N(CH$_2$PO$_3$H$_2$)$_2$ were evaluated by energy-dispersive X-ray (EDX) and SEM elemental mapping analysis (Figure 5). The existence of C, N, O, Fe, and Co elements was confirmed by EDS analysis in MIL-88B(Fe$_2$/Co)-NH$_2$ (Figure 5a). Also, postmodification of bimetal−MOFs with phosphorous acid, the presence of P together with other elements, was approved in Figure 5b. The analysis of mapping shows the uniform distribution of elements on the surface of the MIL-88B(Fe$_2$/Co)-N(CH$_2$PO$_3$H$_2$)$_2$ by SEM elemental mapping analysis (Figure 5c).

N$_2$ adsorption/desorption isotherms of MIL-88B(Fe$_2$/Co)-N(CH$_2$PO$_3$H$_2$)$_2$ were measured, and the results are presented in Figure 6a. The calculated specific surface area based on the BET equation and the total pore volume for MIL-88B(Fe$_2$/Co)-N(CH$_2$PO$_3$H$_2$)$_2$ are 68.2 m^2 g^{-1} and 0.466 cm^3 g^{-1}, respectively. The pore size distribution of the sample based on the BJH method is shown in Figure 6b. The calculated mean pore diameter of MIL-88B(Fe$_2$/Co)-N(CH$_2$PO$_3$H$_2$)$_2$ is 27.3 nm.

The thermal and structural stability of MIL-88B(Fe$_2$/Co)-N(CH$_2$PO$_3$H$_2$)$_2$ is shown by thermal gravimetric (TG) and differential thermal analysis (DTA) in Figure 7. The first weight loss at <100 °C can be assigned to the evaporation and removal of solvents that are trapped within the porous catalyst. The second weight loss at 350 °C can be assigned to the decomposition of MIL-88B(Fe$_2$/Co)-N(CH$_2$PO$_3$H$_2$)$_2$. There-
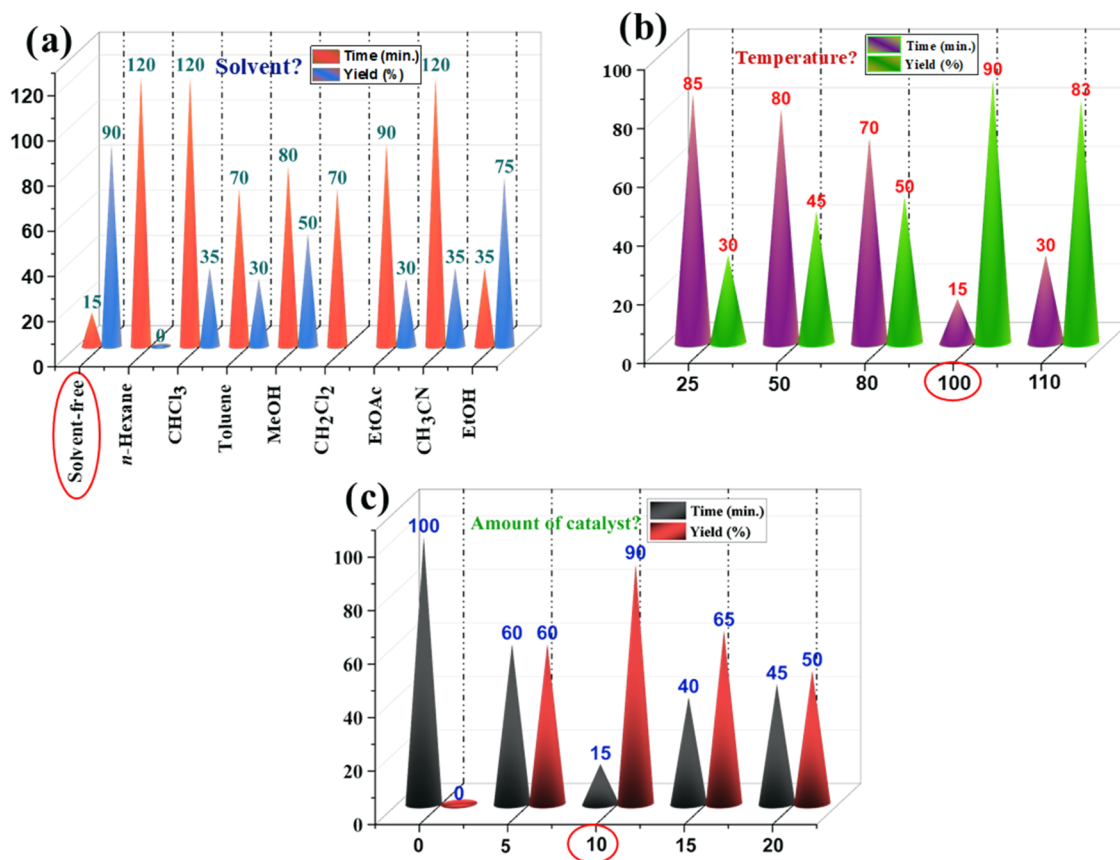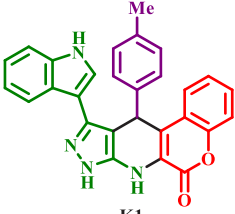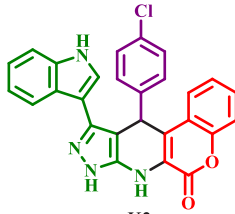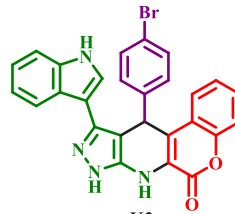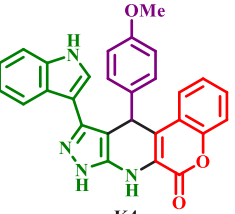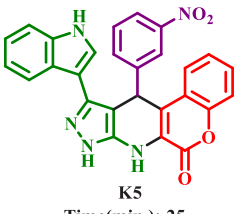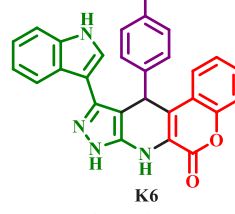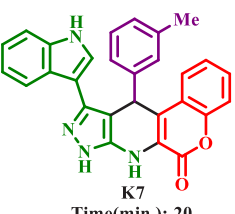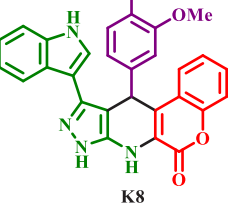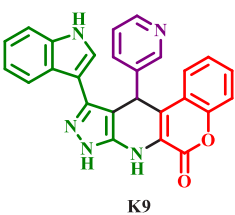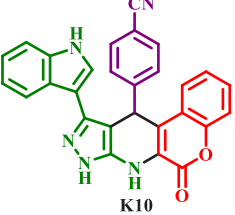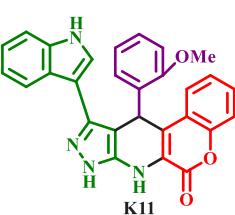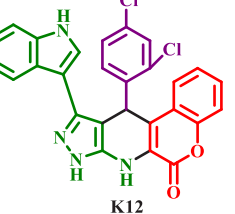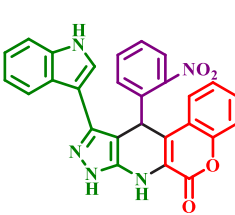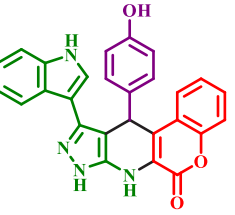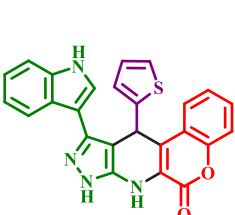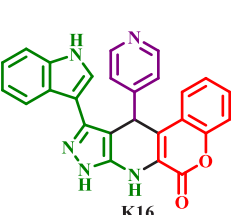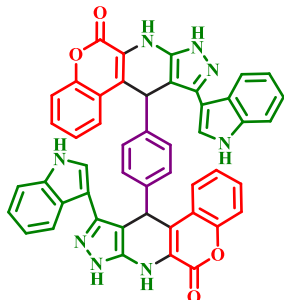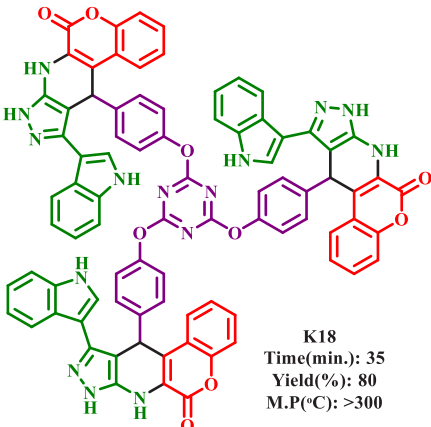

Figure 8. Optimization of some parameter's reaction using MIL-88B(Fe$_2$/Co)-N(CH$_2$PO$_3$H$_2$)$_2$ as a porous catalyst: (a) solvent, (b) temperature, and (c) amount of catalyst.

Table 1. Synthesis of pyrazolo[4,3-*e*]pyridines using MIL-88B(Fe₂/Co)-N(CH₂PO₃H₂)₂ under solvent-free conditions

K1
Time(min.): 20
Yield(%): 87
M.P(°C): >300

K2
Time(min.): 15
Yield(%): 90
M.P(°C): >300

K3
Time(min.): 20
Yield(%): 89
M.P(°C): >300

K4
Time(min.): 20
Yield(%): 90
M.P(°C): >300

K5
Time(min.): 25
Yield(%): 87
M.P(°C): >300

K6
Time(min.): 15
Yield(%): 85
M.P(°C): >300

K7
Time(min.): 20
Yield(%): 85
M.P(°C): >300

K8
Time(min.): 25
Yield(%): 84
M.P(°C): >300

K9
Time(min.): 25
Yield(%): 85
M.P(°C): >300

K10
Time(min.): 15
Yield(%): 90
M.P(°C): >300

K11
Time(min.): 20
Yield(%): 86
M.P(°C): >300

K12
Time(min.): 30
Yield(%): 80
M.P(°C): >300

K13
Time(min.): 25
Yield(%): 85
M.P(°C): >300

K14
Time(min.): 25
Yield(%): 86
M.P(°C): >300

K15
Time(min.): 20
Yield(%): 84
M.P(°C): >300

K16
Time(min.): 20
Yield(%): 87
M.P(°C): >300

K17
Time(min.): 35
Yield(%): 80
M.P(°C): >300

K18
Time(min.): 35
Yield(%): 80
M.P(°C): >300

fore, MIL-88B(Fe₂/Co)-N(CH₂PO₃H₂)₂ is able to catalyze reactions up to 350 °C.

Catalytic Activity. The development of organic methodologies for the synthesis of organic compounds as bioactive

Scheme 3. Proposed mechanism for the synthesis of pyrazolo[4,3-*e*]pyridine using MIL-88B(Fe$_2$/Co)-N(CH$_2$PO$_3$H$_2$)$_2$
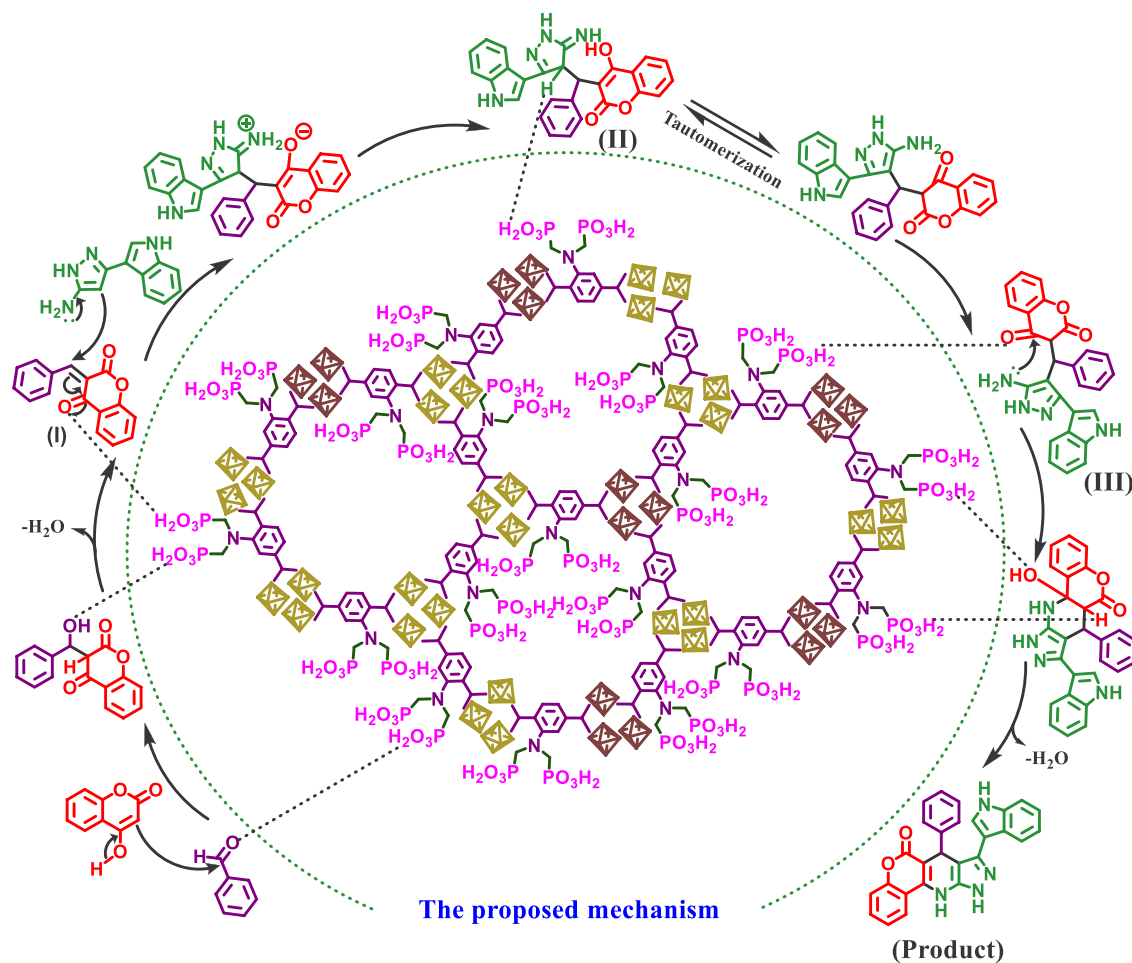
Table 2. Synthesis of pyrazolo[4,3-*e*]pyridine derivatives in the presence of various catalysts

entry	catalyst	amount of catalyst (mol %)	time (min)	yield (%)
1	Fe$_3$O$_4$	10 mg	100	trace
2	CF$_3$SO$_3$H	10	80	25
3	NH$_4$NO$_3$	10	120	-
4	H$_2$SO$_4$	10	120	-
5	FeCl$_3$	10	100	20
6	Fe$_3$O$_4$@Co(BDC)-NH$_2$[35]	10	75	40
7	*p*-TSA	10	90	30
8	SSA[7071]	10 mg	85	25
9	Et$_3$N	10	120	20
10	MHMHPA[50]	10	70	45
11	[PVI-SO$_3$H]FeCl$_4$[71]	10	60	40
12	MIL-100(Cr)/NHEtN(CH$_2$PO$_3$H$_2$)$_2$[30]	10	45	60
13	H$_3$[p(W$_3$O$_{10}$)$_4$].XH$_2$O	10	60	40
14	CQDs[72]	10 mg	45	45
15	APVPB[73]	10 mg	40	30
16	CQDs-N(CH$_2$PO$_3$H$_2$)$_2$/SBA-15[52]	10 mg	45	35
17	Ti-MOF-UR[74]	10 mg	50	55
18	CQDs-N(CH$_2$PO$_3$H$_2$)$_2$[51]	10 mg	35	65
19	Co-MOF-NH$_2$	10 mg	65	35
20	Fe-MOF-NH$_2$	10 mg	40	40
21	MIL-88B(Fe$_2$/Co)-NH$_2$	10 mg	25	55
22	MIL-88B(Fe$_2$/Co)-N(CH$_2$PO$_3$H$_2$)$_2$	10 mg	15	90

candidates has led to extensive research. For this purpose, the synthesis and identification of MIL-88B(Fe$_2$/Co)-N-

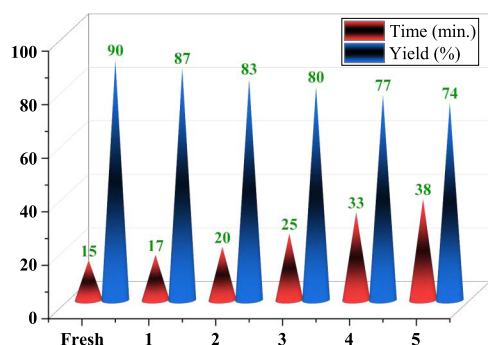(CH$_2$PO$_3$H$_2$)$_2$ as a porous catalyst was investigated in the preparation of pyrazolo[4,3-*e*]pyridine derivatives. To achieve

Figure 9. Recyclability of MIL-88B(Fe$_2$/Co)-N(CH$_2$PO$_3$H$_2$)$_2$ in the synthesis of pyrazolo[4,3-e]pyridine derivatives.

this goal, the reaction among 5-(1H-indol-3-yl)-2H-pyrazol-3-ylamine (1 mmol, 0.198 g), 4-hydroxy-2H-chromen-2-one (1 mmol, 0.162 g), and 4-chlorobenzaldehyde (1 mmol, 0.140 g) was chosen as a model reaction. First, this reaction was evaluated using different solvents such as acetonitrile, n-hexane, methanol, ethanol, toluene, ethyl acetate, chloroform, and dichloromethane, as well as in solvent-free conditions. The results showed that the solvent-free condition has better efficiency (Figure 8a). In another evaluation, the model reaction was investigated at different temperatures and the amounts of catalyst in solvent-free conditions. According to the obtained results, 10 mg of the catalyst and 100 °C is the best reaction condition for the synthesis of desired products (Figure 8b,c).

After the optimal conditions were obtained for the preparation of pyrazolo[4,3-e]pyridine derivatives, various aromatic aldehydes (such as bis, tris-aldehyde, bearing electron-donating and electron-withdrawing groups) were used to synthesize a wide range of desired products (Table 1). The obtained results indicated that MIL-88B(Fe$_2$/Co)-N(CH$_2$PO$_3$H$_2$)$_2$ is appropriate for the preparation of novel target molecules (K1−K18) in high to excellent yields (80−90%) within relatively short reaction times (15−35 min) under mild and green reaction conditions.

In the proposed mechanism, the carbonyl group of aldehydes is activated by MIL-88B(Fe$_2$/Co)-N(CH$_2$PO$_3$H$_2$)$_2$. Then, 4-hydroxy-2H-chroman-2-one reacts with the activated aldehyde, and intermediate (I) is obtained with loss of a H$_2$O molecule (I). In the next step, the 5-(1H-indol-3-yl)-2H-pyrazol-3-ylamine compound is reacted with intermediate (I) as a Michael acceptor to give intermediate (II). In the following, intermediate (II) is converted to intermediate (III) via tautomerization. Finally, intermediate (III) gives the desired product via cyclization with loss of a H$_2$O molecule (Scheme 3).

In another investigation, the efficiency of the catalyst in the preparation of pyrazolo[4,3-e]pyridine derivatives was compared with that of other catalysts. For this purpose, a model reaction of 5-(1H-indol-3-yl)-2H-pyrazol-3-ylamine (1 mmol, 0.198 g), 4-hydroxy-2H-chromen-2-one (1 mmol, 0.162 g), and 4-chlorobenzaldehyde (1 mmol, 0.140 g) was evaluated with organic and inorganic catalysts. The results are shown in Table 2. According to the obtained result, MIL-88B(Fe$_2$/Co)-N(CH$_2$PO$_3$H$_2$)$_2$ as a porous catalyst is suitable for the preparation of pyrazolo[4,3-e]pyridine derivatives. On the other hand, the recyclability of the catalyst was investigated in the model reaction under the above-mentioned optimized reaction conditions. The results are shown in Figure 9. This

catalyst can be reused five times without significant changes in reaction efficiency and reaction time.

CONCLUSIONS

In summary, a bimetallic−organic framework (bimetal−MOF) based on Fe and Co metals with phosphorous acid functional groups was introduced. The simultaneous presence of two metals and phosphorus acid tags in the structure has increased its stability and catalytic activity. The catalytic properties of MIL-88B(Fe$_2$/Co)-N(CH$_2$PO$_3$H$_2$)$_2$ were investigated in the preparation of pyrazolo[4,3-e]pyridine derivatives as biological candidates under mild and green conditions. The significant advantages of the proposed method are high stability, easy separation, environment-friendly nature, recyclability of the catalyst, and clean profile of the reaction.

ASSOCIATED CONTENT

⑤ Supporting Information

The Supporting Information is available free of charge at https://pubs.acs.org/doi/10.1021/acsomega.3c02580.

Spectral data of pyrazolo[4,3-e]pyridine derivatives (PDF)

AUTHOR INFORMATION

Corresponding Authors

Mahmoud Zarei − *Department of Chemistry, Faculty of Science, University of Qom, Qom 37185-359, Iran;* ⓘ orcid.org/0000-0002-3701-9755; Email: mahmoud8103@yahoo.com

Mohammad Ali Zolfigol − *Department of Organic Chemistry, Faculty of Chemistry, Bu-Ali Sina University, Hamedan 6517838683, Iran;* ⓘ orcid.org/0000-0002-4970-8646; Phone: +988138282807; Email: zolfi@basu.ac.ir, mzolfigol@yahoo.com; Fax: +988138380709

Authors

Milad Mohammadi Rasooll − *Department of Organic Chemistry, Faculty of Chemistry, Bu-Ali Sina University, Hamedan 6517838683, Iran*

Hassan Sepehrmansourie − *Department of Organic Chemistry, Faculty of Chemistry, Bu-Ali Sina University, Hamedan 6517838683, Iran*

Mojtaba Hosseinifard − *Department of Energy, Materials and Energy Research Center, Karaj 401602, Iran;* ⓘ orcid.org/0000-0003-3770-5963

Yanlong Gu − *School of Chemistry and Chemical Engineering, Huazhong University of Science and Technology, Wuhan 430074, China;* ⓘ orcid.org/0000-0001-5130-3026

Complete contact information is available at:
https://pubs.acs.org/10.1021/acsomega.3c02580

Notes

The authors declare no competing financial interest.

REFERENCES

(1) Kumar, S.; Jain, S.; Nehra, M.; Dilbaghi, N.; Marrazza, G.; Kim, K. H. Green synthesis of metal−organic frameworks: A state-of-the-

art review of potential environmental and medical applications. *Coord. Chem. Rev.* **2020**, *420*, No. 213407.

(2) Yan, Y.; Gu, P.; Zheng, S.; Zheng, M.; Pang, H.; Xue, H. Facile synthesis of an accordion-like Ni-MOF superstructure for high-performance flexible supercapacitors. *J. Mater. Chem. A* **2016**, *4*, 19078−19085.

(3) Lian, X.; Fang, Y.; Joseph, E.; Wang, Q.; Li, J.; Banerjee, S.; Lollar, C.; Wang, X.; Zhou, H. C. Enzyme−MOF (metal−organic framework) composites. *Chem. Soc. Rev.* **2017**, *46*, 3386−3401.

(4) Liu, C.; Wang, J.; Wan, J.; Yu, C. MOF-on-MOF hybrids: Synthesis and applications. *Coord. Chem. Rev.* **2021**, *432*, No. 213743.

(5) (a) Wang, R.; Xu, H.; Zhang, K.; Wei, S.; Deyong, W. High-quality Al@ Fe-MOF prepared using Fe-MOF as a micro-reactor to improve adsorption performance for selenite. *J. Hazard. Mater.* **2019**, *364*, 272−280. (b) Kumari, A.; Kaushal, S.; Singh, P. P. Bimetallic metal organic frameworks heterogeneous catalysts: Design, construction, and applications. *Mater. Today Energy* **2021**, *20*, No. 100667.

(6) Luz, I.; i Xamena, F. L.; Corma, A. Bridging homogeneous and heterogeneous catalysis with MOFs:"Click" reactions with Cu-MOF catalysts. *J. Catal.* **2010**, *276*, 134−140.

(7) (a) Cai, G.; Yan, P.; Zhang, L.; Zhou, H. C.; Jiang, H. L. Metal−organic framework-based hierarchically porous materials: Synthesis and applications. *Chem. Rev.* **2021**, *121*, 12278−12326. (b) Li, H.; Yang, T.; Fang, Z. Biomass-derived mesoporous Hf-containing hybrid for efficient Meerwein-Ponndorf-Verley reduction at low temperatures. *Appl. Catal., B* **2018**, *227*, 79−89.

(8) Xiao, X.; Zou, L.; Pang, H.; Xu, Q. Synthesis of micro/nanoscaled metal−organic frameworks and their direct electrochemical applications. *Chem. Soc. Rev.* **2020**, *49*, 301−331.

(9) Chakraborty, G.; Park, I. H.; Medishetty, R.; Vittal, J. J. Two-dimensional metal-organic framework materials: Synthesis, structures, properties and applications. *Chem. Rev.* **2021**, *121*, 3751−3891.

(10) Fan, W.; Zhang, X.; Kang, Z.; Liu, X.; Sun, D. Isoreticular chemistry within metal−organic frameworks for gas storage and separation. *Coord. Chem. Rev.* **2021**, *443*, No. 213968.

(11) (a) Suresh, K.; Matzger, A. J. Enhanced drug delivery by dissolution of amorphous drug encapsulated in a water unstable metal−organic framework (MOF). *Angew. Chem., Int. Ed.* **2019**, *58*, 16790−16794. (b) Bae, J.; Lee, C. Y.; Jeong, N. C. Weak Coordination Bond of Chloromethane: A Unique Way to Activate Metal Node Within an Unstable Metal−Organic Framework DUT-34. *Bull. Korean Chem. Soc.* **2021**, *42*, 658−666.

(12) (a) Ni, W.; Zhang, L.; Zhang, H.; Zhang, C.; Jiang, K.; Cao, X. Hierarchical MOF-on-MOF Architecture for pH/GSH-Controlled Drug Delivery and Fe-Based Chemodynamic Therapy. *Inorg. Chem.* **2022**, *61*, 3281−3287. (b) Park, S. H.; Peralta, R. A.; Moon, D.; Jeong, N. C. Dynamic weak coordination bonding of chlorocarbons enhances the catalytic performance of a metal−organic framework material. *J. Mater. Chem. A* **2022**, *10*, 23499−23508.

(13) Ren, J.; Huang, Y.; Zhu, H.; Zhang, B.; Zhu, H.; Shen, S.; Tan, G.; Wu, F.; He, H.; Lan, S.; Xia, X.; Liu, Q. Recent progress on MOF-derived carbon materials for energy storage. *Carbon Energy* **2020**, *2*, 176−202.

(14) Hou, C. C.; Wang, Y.; Zou, L.; Wang, M.; Liu, H.; Liu, Z.; Wang, H. F.; Li, C.; Xu, Q. A Gas-Steamed MOF Route to P-Doped Open Carbon Cages with Enhanced Zn-Ion Energy Storage Capability and Ultrastability. *Adv. Mater.* **2021**, *33*, No. 2101698.

(15) Sepehrmansourie, H.; Alamgholiloo, H.; Pesyan, N. N.; Zolfigol, M. A. A MOF-on-MOF strategy to construct double Z-scheme heterojunction for high-performance photocatalytic degradation. *Appl. Catal., B* **2023**, *321*, No. 122082.

(16) Sepehrmansourie, H.; Alamgholiloo, H.; Zolfigol, M. A.; Pesyan, N. N.; Rasooll, M. M. Nanoarchitecting a Dual Z-Scheme Zr-MOF/Ti-MOF/g-C₃N₄ Heterojunction for Boosting Gomberg−Buchmann−Hey Reactions under Visible Light Conditions. *ACS Sustainable Chem. Eng.* **2023**, *11*, 3182−3193.

(17) Berijani, K.; Morsali, A. Dual activity of durable chiral hydroxyl-rich MOF for asymmetric catalytic reactions. *J. Catal.* **2019**, *378*, 28−35.

(18) Dybtsev, D. N.; Bryliakov, K. P. Asymmetric catalysis using metal-organic frameworks. *Coord. Chem. Rev.* **2021**, *437*, No. 213845.

(19) Adam, R.; Mon, M.; Greco, R.; Kalinke, L. H.; Vidal-Moya, A.; Fernandez, A.; Winpenny, R. E. P.; Doménech-Carbó, A.; Leyva-Pérez, A.; Armentano, D.; Pardo, E.; Ferrando-Soria, J. Self-assembly of catalytically active supramolecular coordination compounds within metal−organic frameworks. *J. Am. Chem. Soc.* **2019**, *141*, 10350−10360.

(20) Yang, J.; Dai, D.; Cai, Z.; Liu, Y. Q.; Qin, J. C.; Wang, Y.; Yang, Y. W. MOF-based multi-stimuli-responsive supramolecular nanoplatform equipped with macrocycle nanovalves for plant growth regulation. *Acta Biomater.* **2021**, *134*, 664−673.

(21) Lu, G.; Chu, F.; Huang, X.; Li, Y.; Liang, K.; Wang, G. Recent advances in Metal-Organic Frameworks-based materials for photocatalytic selective oxidation. *Coord. Chem. Rev.* **2022**, *450*, No. 214240.

(22) Fang, R.; Dhakshinamoorthy, A.; Li, Y.; Garcia, H. Metal organic frameworks for biomass conversion. *Chem. Soc. Rev.* **2020**, *49*, 3638−3687.

(23) Guo, T.; Qiu, M.; Qi, X. Selective conversion of biomass-derived levulinic acid to ethyl levulinate catalyzed by metal organic framework (MOF)-supported polyoxometalates. *Appl. Catal., A* **2019**, *572*, 168−175.

(24) Zhai, Z.; Yan, W.; Dong, L.; Deng, S.; Wilkinson, D. P.; Wang, X.; Zhang, L.; Zhang, J. Catalytically active sites of MOF-derived electrocatalysts: Synthesis, characterization, theoretical calculations, and functional mechanisms. *J. Mater. Chem. A* **2021**, *9*, 20320−20344.

(25) Wen, X.; Guan, J. Recent progress on MOF-derived electrocatalysts for hydrogen evolution reaction. *Appl. Mater. Today* **2019**, *16*, 146−168.

(26) (a) Sepehrmansourie, H. Spotlight: Metal Organic Frameworks (MOFs): As multi-purpose catalysts. *Iran. J. Catal.* **2021**, *11*, 207−215. (b) Sepehrmansourie, H.; Zarei, M.; Zolfigol, M. A.; Babaee, S.; Azizian, S.; Rostamnia, S. Catalytic synthesis of new pyrazolo [3,4-*b*] pyridine via a cooperative vinylogous anomeric-based oxidation. *Sci. Rep.* **2022**, *12*, No. 14145.

(27) Babaee, S.; Zarei, M.; Sepehrmansourie, H.; Zolfigol, M. A.; Rostamnia, S. Synthesis of metal−organic frameworks MIL-101(Cr)-NH₂ containing phosphorous acid functional groups: Application for the synthesis of *N*-Amino-2-pyridone and pyrano[2,3-*c*] pyrazole derivatives via a cooperative vinylogous anomeric-based oxidation. *ACS Omega* **2020**, *5*, 6240−6249.

(28) (a) Tavakoli, E.; Sepehrmansourie, H.; Zarei, M.; Zolfigol, M. A.; Khazaei, A.; Hosseinifard, M. Applications of novel composite UiO-66-NH₂/Melamine with phosphorous acid tags as a porous and efficient catalyst for the preparation of novel spiro-oxindoles. *New J. Chem.* **2022**, *46*, 19054−19061. (b) Danishyar, B.; Sepehrmansourie, H.; Ahmadi, H.; Zarei, M.; Zolfigol, M. A.; Hosseinifard, M. Application of nanomagnetic metal-organic frameworks in the green synthesis of nicotinonitriles via cooperative vinylogous anomeric-based oxidation. *ACS Omega* **2023**, *8*, 18479−18490.

(29) (a) Kalhor, S.; Zarei, M.; Zolfigol, M. A.; Sepehrmansourie, H.; Nematollahi, D.; Alizadeh, S.; Shi, H.; Arjomandi, J. Anodic electrosynthesis of MIL-53(Al)-N(CH₂PO3H₂)2 as a mesoporous catalyst for synthesis of novel (*N*-methyl-pyrrol)-pyrazolo[3,4-*b*] pyridines via a cooperative vinylogous anomeric based oxidation. *Sci. Rep.* **2021**, *11*, No. 19370. (b) Sepehrmansourie, H.; Rasooll, M. M.; Zarei, M.; Zolfigol, M. A.; Gu, Y. Application of metal organic frameworks with sulfonic acid tags in the synthesis of pyrazolo[3,4-*b*]pyridines via a cooperative vinylogous anomeric based oxidation. *Inorg. Chem.* **2023**, *62*, 9217−9229.

(30) Sepehrmansouri, H.; Zarei, M.; Zolfigol, M. A.; Moosavi-Zare, A. R.; Rostamnia, S.; Moradi, S. Multilinker phosphorous acid anchored En/MIL-100(Cr) as a novel nanoporous catalyst for the synthesis of new *N*-heterocyclic pyrimido[4,5-*b*] quinolines. *Mol. Catal.* **2020**, *481*, No. 110303.

(31) Sepehrmansourie, H.; Zarei, M.; Zolfigol, M. A.; Gu, Y. A new approach for the synthesis of bis (3-Indolyl) pyridines via a cooperative vinylogous anomeric based oxidation using ammonium acetate as a dual reagent-catalyst role under mild and green condition. *Polycyclic Aromat. Compd.* 2022, 1−15.

(32) Sepehrmansourie, H.; Kalhor, S.; Zarei, M.; Zolfigol, M. A.; Hosseinifard, M. A convenient catalytic method for preparation of new tetrahydropyrido[2,3-*d*] pyrimidines via a cooperative vinylogous anomeric based oxidation. *RSC Adv.* 2022, 12, 34282−34292.

(33) Ahmadi, H.; Zarei, M.; Zolfigol, M. A. Catalytic Application of a Novel Basic Alkane-sulfonate Metal-organic Frameworks in the Preparation of Pyrido[2,3-*d*] pyrimidines via a Cooperative Vinyl-ogous Anomeric-based Oxidation. *ChemistrySelect* 2022, 7, No. e202202155.

(34) Jalili, F.; Zarei, M.; Zolfigol, M. A.; Khazaei, A. Application of novel metal−organic framework [Zr-UiO-66-PDC-SO₃H]FeCl₄ in the synthesis of dihydrobenzo[*g*]pyrimido[4,5-*b*]quinoline deriva-tives. *RSC Adv.* 2022, 12, 9058−9068.

(35) Sepehrmansourie, H.; Zarei, M.; Zolfigol, M. A.; Babaee, S.; Rostamnia, S. Application of novel nanomagnetic metal−organic frameworks as a catalyst for the synthesis of new pyridines and 1,4-dihydropyridines via a cooperative vinylogous anomeric based oxidation. *Sci. Rep.* 2021, 11, No. 5279.

(36) Naseri, A. M.; Zarei, M.; Alizadeh, S.; Babaee, S.; Zolfigol, M. A.; Nematollahi, D.; Arjomandi, J.; Shi, H. Synthesis and application of [Zr-UiO-66-PDC-SO₃H]Cl MOFs to the preparation of dicyano-methylene pyridines via chemical and electrochemical methods. *Sci. Rep.* 2021, 11, No. 16817.

(37) Babaee, S.; Zarei, M.; Zolfigol, M. A. MOF-Zn-NHC as an efficient *N*-heterocyclic carbene catalyst for aerobic oxidation of aldehydes to their corresponding carboxylic acids via a cooperative geminal anomeric based oxidation. *RSC Adv.* 2021, 11, 36230−36236.

(38) McKinlay, A. C.; Morris, R. E.; Horcajada, P.; Férey, G.; Gref, R.; Couvreur, P.; Serre, C. BioMOFs: metal−organic frameworks for biological and medical applications. *Angew. Chem., Int. Ed.* 2010, 49, 6260−6266.

(39) Yang, X. L.; Ding, C.; Guan, R. F.; Zhang, W. H.; Feng, Y.; Xie, M. H. Selective dual detection of H₂S and Cu²⁺ by a post-modified MOF sensor following a tandem process. *J. Hazard. Mater.* 2021, 403, No. 123698.

(40) Dou, J.; Zhu, C.; Wang, H.; Han, Y.; Ma, S.; Niu, X.; Li, N.; Shi, C.; Qiu, Z.; Zhou, H.; Bai, Y.; Chen, Q. Synergistic Effects of Eu-MOF on Perovskite Solar Cells with Improved Stability. *Adv. Mater.* 2021, 33, No. 2102947.

(41) Zheng, W.; Bi, W.; Gao, X.; Zhang, Z.; Yuan, W.; Li, L. A nickel and cobalt bimetal organic framework with high capacity as an anode material for lithium-ion batteries. *Sustainable Energy Fuels* 2020, 4, 5757−5764.

(42) Dong, S.; Li, Z.; Fu, Y.; Zhang, G.; Zhang, D.; Tong, M.; Huang, T. Bimetal-organic framework Cu-Ni-BTC and its derivative CuO@NiO: Construction of three environmental small-molecule electrochemical sensors. *J. Electroanal. Chem.* 2020, 858, No. 113785.

(43) El-Dafrawy, S. M.; Salama, R. S.; El-Hakam, S. A.; Samra, S. E. Bimetal-organic frameworks (Cuₓ-Cr₁₀₀₋ₓ−MOF) as a stable and efficient catalyst for synthesis of 3,4-dihydropyrimidin-2-one and 14-phenyl-14H-dibenzo [a, j] xanthene. *J. Mater. Res. Technol.* 2020, 9, 1998−2008.

(44) Wu, Y.; Song, X.; Xu, S.; Chen, Y.; Oderinde, O.; Gao, L.; Wei, R.; Xiao, G. Chemical fixation of CO₂ into cyclic carbonates catalyzed by bimetal mixed MOFs: the role of the interaction between Co and Zn. *Dalton Trans.* 2020, 49, 312−321.

(45) Raza, N.; Kumar, T.; Singh, V.; Kim, K. H. Recent advances in bimetallic metal-organic framework as a potential candidate for supercapacitor electrode material. *Coord. Chem. Rev.* 2021, 430, No. 213660.

(46) Li, S.; Gao, Y.; Li, N.; Ge, L.; Bu, X.; Feng, P. Transition metal-based bimetallic MOFs and MOF-derived catalysts for electro-chemical oxygen evolution reaction. *Energy Environ. Sci.* 2021, 14, 1897−1927.

(47) Soni, I.; Kumar, P.; Jayaprakash, G. K. Recent advancements in the synthesis and electrocatalytic activity of two-dimensional metal−organic framework with bimetallic nodes for energy-related applications. *Coord. Chem. Rev.* 2022, 472, No. 214782.

(48) Jalili, F.; Zarei, M.; Zolfigol, M. A.; Rostamnia, S.; Moosavi-Zare, A. R. SBA-15/PrN (CH₂PO₃H₂)₂ as a novel and efficient mesoporous solid acid catalyst with phosphorous acid tags and its application on the synthesis of new pyrimido[4,5-*b*]quinolones and pyrido[2,3-*d*] pyrimidines via anomeric based oxidation. *Microporous Mesoporous Mater.* 2020, 294, No. 109865.

(49) Zarei, M.; Zolfigol, M. A.; Moosavi-Zare, A. R.; Noroozizadeh, E.; Rostamnia, S. Three-Component Synthesis of Spiropyrans Using SBA-15/En Bonded Phosphorous Acid [SBA-15/Pr-NH₁₋ᵧ(CH₂PO₃H₂)ᵧ-Et-NH₂₋ₓ(CH₂PO₃H₂)ₓ] as a New Nanoporous Heterogeneous Catalyst. *ChemistrySelect* 2018, 3, 12144−12149.

(50) Afsar, J.; Zolfigol, M. A.; Khazaei, A.; Zarei, M.; Gu, Y.; Alonso, D. A.; Khoshnood, A. Synthesis and application of melamine-based nano catalyst with phosphonic acid tags in the synthesis of (3-indolyl) pyrazolo [3,4-*b*] pyridines via vinylogous anomeric based oxidation. *Mol. Catal.* 2020, 482, No. 110666.

(51) Rasooll, M. M.; Zarei, M.; Zolfigol, M. A.; Sepehrmansourie, H.; Omidi, A.; Hasani, M.; Gu, Y. Novel nano-architectured carbon quantum dots (CQDs) with phosphorous acid tags as an efficient catalyst for the synthesis of multisubstituted 4*H*-pyran with indole moieties under mild conditions. *RSC Adv.* 2021, 11, 25995−26007.

(52) Rasooll, M. M.; Sepehrmansourie, H.; Zarei, M.; Zolfigol, M. A.; Rostamnia, S. Phosphonic acid tagged carbon quantum dots encapsulated in SBA-15 as a novel catalyst for the preparation of *N*-heterocycles with pyrazolo, barbituric acid and indole moieties. *Sci. Rep.* 2022, 12, No. 20812.

(53) Danishyar, B.; Sepehrmansourie, H.; Zarei, M.; Zolfigol, M. A.; As' Habi, M. A.; Gu, Y. Synthesis and application of novel magnetic glycoluril tetrakis (methylene phosphorous acid) as a nano biological catalyst for the preparation of nicotinonitriles via a cooperative vinylogous anomeric-based oxidation. *Polycycle Aromat. Compd.* 2022, 1−21.

(54) Kalhor, S.; Zarei, M.; Sepehrmansourie, H.; Zolfigol, M. A.; Shi, H.; Wang, J.; Arjomandi, J.; Hasani, M.; Schirhagl, R. Novel uric acid-based nano organocatalyst with phosphorous acid tags: Application for synthesis of new biologically-interest pyridines with indole moieties via a cooperative vinylogous anomeric based oxidation. *Mol. Catal.* 2021, 507, No. 111549.

(55) Rasooll, M. M. Phosphorus acid: As multi-purpose catalysts. *Iran. J. Catal.* 2022, 12, 107−113.

(56) Lopes, T. R.; Cipriano, D. F.; Goncalves, G. R.; Honorato, H. A.; Schettino, M. A., Jr; Cunha, A. G.; Emmerich, F. G.; Freitas, J. C. Multinuclear magnetic resonance study on the occurrence of phosphorus in activated carbons prepared by chemical activation of lignocellulosic residues from the babassu production. *J. Environ. Chem. Eng.* 2017, 5, 6016−6029.

(57) (a) Das, S.; Behera, S. S.; Murmu, B. M.; Mohapatra, R. K.; Mandal, D.; Samantray, R.; Parhi, P. K.; Senanayake, G. Extraction of scandium (III) from acidic solutions using organo-phosphoric acid reagents: A comparative study. *Sep. Purif. Technol.* 2018, 202, 248−258. (b) Sato, T.; Watanabe, K.; Nagase, H.; Kito, H.; Niikawa, M.; Yoshioka, Y. Investigation of the hemolytic effects of various organophosphoric acid triesters (OPEs) and their structure-activity relationship. *Environ. Toxicol. Chem.* 1997, 59, 305−313.

(58) Zimmerman, J. B.; Anastas, P. T.; Erythropel, H. C.; Leitner, W. Designing for a green chemistry future. *Science* 2020, 367, 397−400.

(59) Beach, E. S.; Cui, Z.; Anastas, P. T. Green Chemistry: A design framework for sustainability. *Energy Environ. Sci.* 2009, 2, 1038−1049.

(60) Bathla, A.; Younis, S. A.; Pal, B.; Kim, K. H. Recent progress in bimetallic nanostructure impregnated metal-organic framework for photodegradation of organic pollutants. *Appl. Mater. Today* 2021, 24, No. 101105.

(61) Chen, L.; Wang, H. F.; Li, C.; Xu, Q. Bimetallic metal−organic frameworks and their derivatives. *Chem. Sci.* 2020, 11, 5369−5403.

(62) Mishra, A. P.; Bajpai, A.; Rai, A. K. 1,4-Dihydropyridine: A Dependable Heterocyclic Ring with the Promising and the Most Anticipable Therapeutic Effects. *Mini. Rev. Med. Chem.* **2019**, *19*, 1219−1254.

(63) Gündüz, M. G.; Armaković, S. J.; Dengiz, C.; Tahir, M. N.; Armaković, S. Crystal structure determination and computational studies of 1,4-dihydropyridine derivatives as selective T-type calcium channel blockers. *J. Mol. Struct.* **2021**, *1230*, No. 129898.

(64) Singh, T. P.; Singh, O. M. Recent Progress in Biological Activities of Indole and Indole Alkaloids. *Mini Rev. Med. Chem.* **2018**, *18*, 9−25.

(65) Faria, J. V.; Vegi, P. F.; Miguita, A. G. C.; Dos Santos, M. S.; Boechat, N.; Bernardino, A. M. R. Recently reported biological activities of pyrazole compounds. *Bioorg. Med. Chem.* **2017**, *25*, 5891−5903.

(66) Marinescu, M. Synthesis of Antimicrobial Benzimidazole−Pyrazole Compounds and Their Biological Activities. *Antibiotics* **2021**, *10*, No. 1002.

(67) Monfared, A.; Esmaeeli, Z. A One-pot Condensation for Synthesis 2-methyl-4-phenylpyrano [3, 2-*c*] chromen-5(4*H*)-one and Synthesis of Warfarin by Ionic Liquid Catalysis. *Iran. J. Pharm. Res.* **2016**, *15*, No. 343.

(68) El-Mekabaty, A.; Etman, H. A.; Mosbah, A. Synthesis of some new fused pyrazole derivatives bearing indole moiety as antioxidant agents. *J. Heterocycl. Chem.* **2016**, *53*, 894−900.

(69) Wang, J.; Wang, J.; Zhang, M.; Li, S.; Liu, R.; Li, Z. Metal-organic frameworks-derived hollow-structured iron-cobalt bimetallic phosphide electrocatalysts for efficient oxygen evolution reaction. *J. Alloys Compd.* **2020**, *821*, No. 153463.

(70) Zolfigol, M. A. Silica sulfuric acid/NaNO$_2$ as a novel heterogeneous system for production of thionitrites and disulfides under mild conditions. *Tetrahedron* **2001**, *57*, 9509−9511.

(71) Sepehrmansourie, H.; Zarei, M.; Taghavi, R.; Zolfigol, M. A. Mesoporous ionically tagged cross-linked poly (vinyl imidazole) s as novel and reusable catalysts for the preparation of *N*-heterocycle spiropyrans. *ACS Omega* **2019**, *4*, 17379−17392.

(72) Schneider, J.; Reckmeier, C. J.; Xiong, Y.; von Seckendorff, M.; Susha, A. S.; Kasák, P.; Rogach, A. L. Molecular fluorescence in citric acid-based carbon dots. *J. Phys. Chem. C* **2017**, *121*, 2014−2022.

(73) Noroozizadeh, E.; Moosavi-Zare, A. R.; Zolfigol, M. A.; Zarei, M.; Karamian, R.; Asadbegy, M.; Yari, S.; Farida, S. H. M. Synthesis of bis-coumarins over acetic acid functionalized poly (4-vinylpyridinum) bromide (APVPB) as a green and efficient catalyst under solvent-free conditions and their biological activity. *J. Iran. Chem. Soc.* **2018**, *15*, 471−481.

(74) Torkashvand, Z.; Sepehrmansourie, H.; Zolfigol, M. A.; As' Habi, M. A. Application of Ti-MOF-UR as a new porous catalyst for the preparation of pyrazolo [3, 4-*b*] quinoline and pyrazolo [4, 3-*e*] pyridines. *Mol. Catal.* **2023**, *541*, No. 113107.